Modeling the flow and mass transport in a mechanically stimulated parametric porous scaffold under fluid-structure interaction approach

M. Malvè[a,b,c,*], D.J. Bergstrom[d], X.B. Chen[d,e]

[a] *Aragón Institute of Engineering Research. Universidad de Zaragoza, C/María de Luna s/n, E-50018 Zaragoza, Spain*

[b] *CIBER-BBN. Centro de Investigación en Red en Bioingeniería, Biomateriales y Nanomedicina, C/Poeta Mariano Esquillor s/n, E-50018 Zaragoza, Spain*

[c] *Universidad Pública de Navarra. Departamento de Ingeniería, Edificio de los Pinos, Campus Arrosadía s/n, E-31006 Pamplona, Spain*

[d] *Department of Mechanical Engineering, University of Saskatchewan, College of Engineering, Engineering Building 57, Campus Drive, Saskatoon SK, S7N 5A9, Canada*

[e] *Division of Biomedical Engineering, University of Saskatchewan, College of Engineering, Engineering Building 57, Campus Drive, Saskatoon SK, S7N 5A9, Canada*

Abstract

Tissue engineering scaffolds combined with bioreactors are used to cultivate cells with the aim of reproducing tissues and organs. The cultivating process is critical due to the delicate in-vitro environment in which the cells should reproduce. The distribution of nutrients within the engineered construct depend on the scaffold morphology and the analysis of the fluid flow and transport phenomena under mechanical loading when the scaffold is coupled with a bioreactor is crucial for this scope. Unfortunately,

due to the complicated microstructure of the scaffold, it is not possible to perform this analysis with experiments and numerical simulation can help in this sense. In this study we have computed the fluid flow and the mass transport of a parametrized scaffold in perfusion bioreactors analyzing the influence of the microstructure of the scaffold using the fluid-structure interaction approach. The latter allows considering the porous construct as compliant yet determining important structural parameters such as stresses and strains that could be sensed by the cells. The presented model considered flow perfusion that provided nutrients and mechanical compression. In particular, we have studied the effect of controllable parameters such as the diameter of the scaffold strand and the porosity on the mechanical stresses and strains, shear stress and mass transport. The results of this work will help to shed light on the necessary microenvironment surrounding the cultivated cells improving culturing scaffold fabrication.

Key words: Scaffold, mass transfer, bioreactor, tissue engineering, mechanical stimulation, fluid-structure interaction

---

***Corresponding author**:
Mauro Malvè, PhD, Universidad Pública de Navarra. Departamento de Ingeniería, Edificio de los Pinos, Campus Arrosadía, E-31006 Pamplona, Spain
Phone: (+34) 948 16 9294
Fax: (+34) 948 16 9099
Email: `mauro.malve@unavarra.es`

1 Introduction

Cartilage repair tissue engineering aims to cultivate cells by creating adequate microenvironment and culturing strategies *in-vitro*. In recent years, a variety of porous tridimensional scaffolds have been designed for this goal, considering that these structures provide a good architecture for cell culture. In particular, the combined use of bioreactors with three-dimensional (3D) porous structures has provided the necessary conditions for the cells to live and reproduce by means of a variety of stimuli. The latter is crucial for cartilage tissue, which needs a specific mechanical stimulation for maintaining its differentiation in-vitro under different biochemical factors [1].

The scaffold is commonly located in a bioreactor. In this device, oxygen and nutrients continuously flow within the culture medium through the pores of the scaffold, allowing the attached cells to grow and proliferate. In the literature of the field it is stated that the shear stresses on the scaffold due to this fluid motion can positively or adversely affect the culture. While a moderate shear stress could benefit the formation of glycosaminoglycan (GAG) and as a consequence the cartilage tissue repair and growth, on the other side a high shear stress may sweep off the attached cells or cause their apoptosis [2]. For this reason, for the cell culture is crucial to find a compromise between the mass transfer and the shear stress.

Computational fluid dynamics (CFD) has been widely used for solving and determining the shear stress distribution of idealized [3,4] and complex microCT-based scaffold structures [5–12]. Recently, a validation of such models using particle image velocimetry (PIV) has been proposed with the aim of investigating how fluid flow conditions modulate cell motion and deposition during perfusion [13–15]. These models provided insight to the shear stress on the scaffold-attached cells and to investigated global characteristics such as porosity and permeability, but neglect the mass transport phenomena that, on the contrary, is included in other studies [16–23]. Computational modeling has been applied also under pure structural finite element analysis to predict the mechanical stimulation experienced within tissue engineered scaffolds due to mechanical compression/stretching *in vitro* [24–26]. The finite elements method (FEM) offers the possibility of handling complex geometry such homogeneous or non-homogeneous microstructures and analyzing the scaffold architectures [7,24,5,27,28].

It is known that cartilage reconfigures both *in vivo* and *in vitro* in response to mechanical loads [6,29]. For this reason, mechanical stimulation is believed to be a potential tool for modulating extra-cellular matrix synthesis in tissue-engineered cartilage [30]. Thus, apart from the fluid motion, another important parameter to take into account for cell culturing is the mechanical load applied to the scaffold. *In vitro* studies on cartilage cultures have demonstrated that static loading generally inhibits glycosaminoglycan (GAG) synthesis [31], while cyclic loading can increase or suppress GAG synthesis, depending on the load frequency [31–33], amplitude [34] and duration of load application [33]. In cartilage tissue engineering studies for cell-seeded scaffolds, the effects of the frequency of dynamic loading have been studied over a wide range of frequencies in conjunction with factors such as cell seeding density [35] and loading configuration [36] with the aim of measuring the regeneration of the extra cellular matrix over the culture time period [29]. From these studies we can conclude that a dynamic mechanical loading of articular cartilage massively affects the regulatory pathways by which chondrocytes respond to their surroundings [37]. Only a few recent studies have attempted to compute fluid perfusion through

the scaffold labyrinth and mass transfer phenomena considering the effective micro-architecture of the scaffold because of the computational time required for such analyses, especially when further combined with fluid-structure interaction (FSI) [23,27,38–40]. Although mass transfer in porous medium such as a tissue engineering scaffold has attracted much attention for providing the correct environment for cells to reproduce, its analysis is incomplete and further knowledge is necessary. A few works oriented to oxygen consumption have proposed mass transport models for this kind of application [23,41–43]. Other studies characterized the porosity and mass transport properties of polyurethane non-regular scaffolds [44,45].

For reproducing *in silico* the microenvironment within cartilage tissues by means of *in vitro* models, the evaluation of the conditions surrounding a cell at a given flow rate in a certain location of the scaffold represents essential information. As discussed, mechanical stimuli depend on both fluid motion and scaffold structural loading. For this reason, the presented work analyzes in detail the flow within a scaffold under mechanical stimulation as a function of the structural parameters of the scaffold. In addition, the analysis of the mass transport in each architecture is provided. The scaffold considered in this work is a manufactured structure that has been fabricated by means of rapid prototyping (RP) techniques and has the advantage that its microstructure is regular and controllable so that the geometry can be modeled by CAD methods. For this device, a study of the effect of parameters such as the diameter of the scaffold strand and the scaffold porosity on the shear stress in the fluid, on the structural stresses and strains, and mass transport within the scaffold is proposed. Such knowledge will help to improve scaffold design, fabrication and culturing strategies.

2 Materials and Methods

2.1 Scaffold and bioreactor configuration

The scaffold structure used in this work has been already described in details in a previous study [9] so that here only a general overview is given. Its design consists of a regular distribution of cylindric strands with variable diameter and spacing between elements (Figure 1). The diameter and height of the scaffold are 3 mm and 5 mm, respectively. Each layer of elements is organized by an offset of $\theta = 90°$ in their orientation from layer to layer.

The scaffold architecture can be described by means of two parameters that can be controlled during the scaffold fabrication [46,47]: the strand diameter (D) and the horizontal span(Y).

These parameters with the distance between two adjacent horizontal (h_{xy}) and vertical (h_z) strands, represent the pore sizes sketched in the Figure 1. In previous research [46], the vertical pore size (h_z) has been described as a function of geometrical and material properties of the scaffold i.e. the diameter of the strand (D), the density of the scaffold material (ρ), the material elastic limit stress (σ_e), the horizontal span (Y) and the angle between two consecutive layers (θ) (see Figure 1). On the contrary, the horizontal distance (h_{xy}) is exclusively associated with the strand diameter (D) and the horizontal span (Y). The approximate relationship can be described as follows:

$$h_z = D \cdot \sqrt{1 - \frac{\rho g Y}{2\sigma_e} \cdot sin\theta} \tag{1}$$

As in previous studies [46,9] the scaffold is fabricated using a chitosan solution with 40% hydroxylapatite (HA) gel with an elastic limit stress of $\sigma_e = 11.0\ Pa$. In the present study, the strand diameter D was varied from 0.2 to 0.4 mm, while the horizontal span Y was varied from 0.5 to 0.9 mm. As a function of the parameters Y and D we considered 9 different scaffolds that are classified in the Table 1. The vertical pore sizes corresponding to each scaffold are given in Table 2. With this information, the geometrical model was carried out by means of the software Rhineceros (Robert McNeel and Associates). From the geometrical model, the porosity, which is defined as the ratio of the void volume to the total volume, was calculated for each scaffold (see Table 2). As mentioned, for reason of computational costs, unlike the study in [9], only a cylindrical sample of the entire scaffold was considered. The bioreactor consists of a cylindrical tube of 50 mm length and with the same diameter as the scaffold.

The computational model was implemented using the software package Adina *R&D* (Adina Inc., Watertown, MA, USA) with the aim of evaluating the the wall shear stress, the stresses and strains and the mass transport within the porous scaffold structure considering the fluid-structure interaction. The cell culture media consisted of water and dissolved nutrients so that it was considered as incompressible, homogeneous and Newtonian with a density of 1000 kg/m^3 and a viscosity of 0.001 $Pa\ s$ [10]. For the FSI model we considered the structure of the scaffold to be made of a homogeneous, isotropic and elastic material [7,23,48].

The FSI simulations were performed assuming quasi-steady condition for the flow model and static condition for the solid model under a residual convergence criteria of 10^{-4}.

2.2 Boundary conditions

The scaffold structure was considered as deformable. Its elastic modulus was set to 0.4 MPa [49,50]. As mechanical stimulation, a uniaxial compression with a maximum strain of 5% was applied. This compressive strain is similar to that encountered inside the human body (which is less than 6% [51]). The latter was mimicked by means of a uniform displacement equivalent to a uniaxial strain of 5% applied on the nodes of the upper side of the meshes while fixing the nodes of the lower side [7].

Regarding the necessary fluid flow to be provided, low velocity may increase cell proliferation while peaks of high velocity are associated with cell apoptosis. However, high levels of fluid velocity are necessary for cell seeding within the scaffolds [7]. In this context, it is clear that a compromise is required [2]. Considering that an increase of flow promotes an increase of wall shear stress (WSS) within the scaffold elements as evaluated in [9], we considered only one flow condition of 0.05 ml/min. The latter was adapted to the inlet diameter of the present study that is smaller than that designed in [9].

For the outlet boundary condition, as usual for fluid-structure interaction models, pressure conditions should be prescribed. Generally speaking, for correctly computing the stresses and strains, flow/velocity-pressure conditions are required. Since we imposed the flow at the inlet and the pressure at the outlet was unknown, we performed a CFD analysis of the fluid domain imposing the flow at both inflow and outflow. Once the pressure was determined, we used its value as outlet condition for the FSI model [27]. The bioreactor walls were considered as rigid and a no-slip boundary condition was applied. The surface of the porous construct that represented the fluid-solid interface was also affected by the no-slip condition.

For modeling the mass transport within the scaffold, in the commercial software, the mass transport equation was added and solved with the classical Navier-Stokes equations (for details see [52]). We used a diffusivity constant of 9.4×10^{-4} mm^2/s that corresponds to the glucose diffusivity in water [45]. As boundary conditions we considered a mass ratio of 0.5 on the scaffold surface, indicating a concentration of 50% glucose in water, the same mass ratio at the inlet, considering that the flow continuously provides nutrients, a zero gradient at the outlet and zero at the walls of the bioreactor.

The fluid and solid models were meshed with a non-uniform unstructured grid in which the element size was varied depending on the part of the scaffold and of the bioreactor. Local grid refinements were used to resolve the microstructure of the scaffold geometry. In addition, as usual, in order to guarantee mesh independent results, a grid independence study was carried out. This study was performed on the rigid model to reduce the computational costs. We considered three different meshes of increasing size. In particular, three grids of approximatively $0.8 \cdot 10^6$, $1.6 \cdot 10^6$ and $3.2 \cdot 10^6$ elements were analyzed. The difference in the calculated maximum wall shear stresses between the last two meshes was approximately 2%. Therefore, the grid containing $1.6 \cdot 10^6$ elements was assumed to be fine enough to accurately compute the flow features and the WSS within the scaffold. The solid model was created simultaneously to the fluid so that the structure of the scaffold was forced to be discretized with the number of elements selected by the fluid model. In this way, coincident nodes between fluid and solid mesh were assessed on the fluid-structure interface. The final structural mesh was composed by $0.8 \cdot 10^6$ elements. The mesh sizes were kept approximatively constant for all simulated cases.

3 Results

Figure 2 shows the simulation results for the case of scaffold $SC1-3$ corresponding to $Y = 0.5\ mm$ and $D = 0.4\ mm$. Note that the fluid dynamics results presented with velocity arrows are qualitatively similar for all the scaffold configurations so that, in this sense, the selected scaffold can be considered representative. The velocity maps around the scaffold calculated by means of the FSI model indicate the direction of fluid motion inside the microstructure of the scaffold. The fluid penetrates inside the scaffold from the frontal surface of the porous construct, and exits from the back surface but also from the side pores. The flow tends to go through the tissue scaffold causing a strong perfusion inside the microstructure. In contrast, as shown in the Figure 3-(a), there is minimal fluid motion in other areas of the bioreactor. Of course, according to the scaffold stiffness, the compression promotes or contributes to the fluid flow within the pores. The strong perfusion highlighted produces relatively high shear stresses on the surfaces of the scaffold. Especially in the regions near the outer edge, due to the separation of the flow from the construct strands, the WSS is particularly high (Figure 3-(b)). The latter suggests that cells seeded near these regions may be affected by higher WSS compared to the central regions

of the microstructure. This finding has implications in the cell strategy: in fact, for avoiding regions affected by high shear stress the cells should be located in the centre area of the scaffold as previously found by other authors [9,13].

Figure 3-(c) shows the pressure distribution within the scaffold. As expected the pressure is very low due to the reduced inflow considered in this work. The pressure drastically decreases by around two orders of magnitude along the longitudinal direction from the inlet to the outlet. As expected, the scaffold promotes a significative pressure drop inside the bioreactor that depends again on the controllable parameters. The pressure drop decreases with increasing porosity i.e. increasing span size Y and/or decreasing strand diameter D. The overall computed pressure drops are summarized for all the cases studied in Table 3.

The longitudinal strain spatial distribution inside the scaffold is depicted in the Figure 4 by means of the major principal strain. This distributions is not uniform, as visible in the figure. The scaffold strain computed by the FSI model is maximum in the longitudinal direction, due to the applied boundary condition. However, it is sufficiently low, indicating a small pore deformation and suggesting that the scaffold remains within the linear elastic region. The maximum stress promoted by the applied strain and by the pressure difference imposed by the flow is 45.59 kPa in compression. As depicted in the Figure 4, higher strains appear in the regions near the strands connections. The stress depends only on the strain applied to the model and on the porosity; a decrease in porosity, promotes an increase in stiffness of the construct [53]. The scaffold material is almost rigid for the low fluid flow so that the contribution of the pressure drop to the compressive stresses is limited. However, from the computations it is visible that regions with higher strains are located in the contact region between scaffold segments. On the contrary, low strains are visible on the top surface where the strain is applied and on the bottom where the model is constrained. Considering that the scaffold architectures are also affected by high WSS, the computation of strains and stresses reinforces the strategy to seed cells in the central regions of the scaffold. The results suggest in fact a different combination of mechanical stimuli for cells. The scaffold shows variable compression strain stimuli and fluid shear stress stimuli at different locations. In particular, different regions are subjected to a high level of only one of these stimuli as previously found by other authors [7].

The change in WSS, maximum principal stress and the pressure drop are shown in the Figure 5 as a function of the different considered scaffold. The maximum principal stress follows a similar tendency with respect to the WSS. It decreases with increasing strand diameter while globally decreasing when the span Y increases. The pressure also follows a similar trend. As discussed, the pressure increases with increasing porosity. In the Figure 6-a) and -b), the dependence of the

maximal shear stress and of the compressive major principal stress for scaffolds with different values of D and Y, respectively, is depicted. The tendencies shown suggest that architectures with a smaller strand diameter D can be used for limiting the wall shear stress and the major principal stress levels within the scaffold. In addition, the horizontal span Y can be used to regulate both stress levels within the scaffold.

Finally we have computed the mass transport within the scaffold microstructure with the aim to analyze the qualitative distribution of concentration of nutrients inside the scaffold. This distribution is reported in the Figure 7 for the scaffold $SC1-3$. The concentration of nutrients was found qualitatively similar in all considered scaffolds, even though the mass transport in a porous construct depends on the porosity and thus on the pressure drop as documented in [45]. Depending on the span Y and strand diameter D, the pore size of the scaffold changes so that the mass transport varies even slightly as the pressure drop increase or decrease. The mass transport distribution is not completely uniform especially in the vicinity of the scaffold periphery. The latter reinforces the necessity of seeding the cells in the central regions of the scaffold especially for avoiding critical regions such as the locations between the scaffold and bioreactor.

4 Discussion

In this study, the fluid flow and mass transport with a mechanical stimulation on regular scaffolds was studied by means of a fluid-structure interaction approach. The flow through scaffolds in bioreactors can be defined as a system which is composed of a porous media and a homogenous fluid. The latter is related to flows with simple geometries, for example flow over a porous layer or flow through a porous plug [41,42]. The small samples presented here allowed for an accurate evaluation of the scaffold microstructure flow conditions and deformation that may help to understand their effect on the local seeded cells. We have computed the flow and velocity field and the WSS distributions for the entire domain, taking into account a simple geometry for the bioreactor and variable scaffold architectures. In addition, we have considered the scaffold structure as compliant thus allowing the computation of the tensile stresses on the microstructure. These stresses are mainly due to the mechanical stimulus applied on the scaffold, that is responsible for the cell differentiation, rather than the flow, that supply nutrients to seeded cells. The microstructure considered in this work possess some controllable parameters that were varied for studying their effect on the WSS, on the tensile stresses and on the pressure drop.

Previous studies oriented their investigation on only CFD models for analyzing these type of variables that cannot be assessed by means of experiments [6–11,15,13,14,12]. Only recent works apply the FSI technique for studying the complex hydrodynamic environment within a scaffold [23,27,38–40]. Most of these studies are oriented to bone tissue engineering. Some authors highlight how the flow can affect the osteocytes seeded in a regular scaffold [27,38] or study the nature of the mechanical stimulus applied to a single cell [40]. Our study, oriented to cartilage tissue engineering, shows that the WSS depends on the location within the scaffold, being normally higher in the periphery and lower in the central regions of the scaffold. The WSS seems to depend on the span Y and strand diameter D, confirming previous results found through a comprehensive CFD study [9]. As we showed, especially an increase of D promotes higher shear stress so that the parameter should be kept low to limit the risk of removing the cells from these regions. Also the horizontal span can be used to adjust the shear stress level within the scaffold, in this case, a larger span results in a reduction of the WSS. Furthermore, we have provided a spatial map of the stresses, of the strains and of WSS that may improve seeding strategies which are normally based separately only on the shear stress or on the strains computed in the scaffold. As expected we have seen that the stresses on the scaffold architecture are manly due to the applied strain while the contribution of the flow is generally negligible. The maximal stress value on the scaffold increases for increasing strand diameter D for each strand Y, but tends to decrease for increasing span Y for each D.

Within the FSI model, it was also possible to predict low flow areas and flow recirculation in the vicinity of the scaffold cells that may result in reduced cell stimulation in these areas and have important implications for nutrient transport through the scaffold, as stated in the literature [27]. In particular, in these regions, the concentration of the nutrients is low so that the overall concentration within the structure is not uniform. However, since it is not possible to control the exact distribution of the cells inside the scaffold, a homogeneous nutrient concentration is highly desirable. Nevertheless, only a few studies have analyzed the mass transfer within a scaffold. These works were oriented to the oxygen consumption [41,42,23] and nutrient transport [44,45]. The association of the scaffold with the bioreactor should theoretically provide a suitable environment which includes efficient nutrient delivery, waste removal, and mechanical stimulation [42]. In this view, the described computational approach may be useful for improving the understanding of the shear stresses and mass transport generated in a scaffold during mechanical stimulation and can be extended to other bioreactors or scaffold types.

Limitations of this work regard first of all the considered flow steadiness. As documented in the literature [13] pulsatile flows can be more stimulatory than steady flows. In addition, different

mechanical stimulations should be tested since a specific level for the required strain has not yet been found and depends on the application. Also, in further investigation, a cyclic strain, neglected in this analysis, should be considered. Finally, the study of mass transport that can provide additional useful information for the seeded cells needs to be improved and an overall experimental validation would be necessary for assessing the reliability of the computational model.

Future work and developments in this field may include a variable time-dependent stimulation, a non-regular scaffold architecture with consequent changes in terms of porosity, permeability, dimensions of pores, nutrient transport and shear stress acting on the cells.

5 Conclusions

In this study we have investigated the fluid flow and the mass transport inside and around a scaffold within a bioreactor in the presence of mechanical stimulation. The results show that the value of the strand diameter and horizontal span influence the wall shear stress generated on the scaffold. In this sense, we found that the compliance of the scaffold has a low effect. Generally, with an increase in the diameter, the maximal wall shear stress increased; with an increase in the horizontal span, the wall shear stress decreased. The maximum principal stress seems to follow the same trend. Depending on the strain imposed on the microstructure, generally, an increase of porosity promotes a reduction of the necessary compression stresses for reaching the same level of deformation. The nutrient distribution within the porous construct was computed analyzing the mass transport in the cell culture and it was found that it is influenced by the scaffold microstructure as found by other authors. The concentration of nutrients and the WSS suggest to seed cells in the center region of the scaffold avoiding the periphery of the construct. As a conclusion, this work may help to increase the knowledge of the fluid flow and mass transport within a scaffold cultured in a bioreactor. The effects of the controllable factors such those of the scaffold microstructure may be useful in the future for optimizing the scaffold design for different applications such as further complex numerical studies and especially for novel experimental set-up in the field.

Acknowledgments

The authors acknowledge the financial supports to this project from the Spanish Ministry of Education, Culture and Sport via the National Program "Salvador de Madariaga" (PRX17/00335) and the Saskatchewan Health Research Foundation via the Health Research Group Program (SHRF Reference #2784). Also, the authors thank the CIBER-BBN financed by the Instituto de Salud Carlos III and the Spanish Ministry of Education, Industry and Competitiveness via the research project (DP12017-83259-R)

Conflict of Interest

None of the authors of this work has conflict of interest with other people and organizations.

References

[1] U. Meyer, A. Büchter, N. Nazer, H. P. Wiesmann, Design and performance of a bioreactor system for mechanically promoted three-dimensional tissue engineering, British Journal of Oral and Maxillofacial Surgery 44 (2006) 134–140.

[2] S. H. Cartmell, B. D. Porter, A. J. Garcia, R. E. Guldberg, Effects of medium perfusion rate on cell-seeded three-dimensional bone constructs in vitro, Tissue Engineering 9 (2003) 1197–1203.

[3] M. T. Raimondi, F. Boschetti, L. Falcone, G. B. Fiore, A. Remuzzi, E. Marinoni, M. Marazzi, R. Pietrabissa, Mechanobiology of engineered cartilage cultured under a quantified fluid-dynamic environment, Biomechanics and Modeling in Mechanobiology 1 (2002) 69–82.

[4] F. Boschetti, M. T. Raimondi, F. Migliavacca, G. Dubini, Prediction of the micro-fluid dynamic environment imposed to three-dimensional engineered cell systems in bioreactors, Journal of Biomechanics 39 (2006) 418–425.

[5] B. Porter, R. Zauel, H. Stockman, R. Guldberg, D. Fyhrie, 3-D computational modeling of media flow through scaffolds in a perfusion bioreactor, Journal of Biomechanics 38 (2005) 543–549.

[6] M. Cioffi, F. Boschetti, M. T. Raimondi, G. Dubini, Modeling evaluation of the fluid-dynamic microenvironment in tissue-engineered constructs: a micro-CT based model, Biotechnology and Bioengineering 93 (3) (2006) 500–510.

[7] C. Sandino, J. A. Plannel, D. Lacroix, A finite element study of mechanical stimuli in scaffolds for bone tissue engineering, Journal of Biomechanics 41 (2008) 1005–1014.

[8] M. T. Raimondi, M. Moretti, M. Cioffi, C. Giordano, F. Boschetti, K. Lagana, R. Pietrabissa, The effect of hydrodynamic shear on 3D engineered chondrocyte systems subject to direct perfusion, Biorheology 43 (2006) 215–222.

[9] X. Yan, X. B. Chen, D. J. Bergstrom, Modeling of the Flow within Scaffolds in Perfusion Bioreactors, American Journal of Biomedical Engineering 1 (2) (2015) 72–77.

[10] V. Acosta-Santamaría, M. Malvè, A. Duizabo, A. Mena-Tobar, G. Gallego-Ferrer, J. M. García-Aznar, M. Doblaré, I. Ochoa, Computational Methodology to Determine Fluid Related Parameters of Non Regular Three-Dimensional Scaffolds, Annals of Biomedical Engineering 41 (11) (2013) 2367–2380.

[11] E. Zermatten, J. R. Vetsch, D. Ruffoni, S. Hofmann, R. Möller, A. Steinfeld, Micro-computed tomography based computational fluid dynamics for the determination of shear stresses in scaffolds within a perfusion bioreactor, Annals of Biomedical Engineering 42 (5) (2014) 1085–1094.

[12] A. Campos Marin, M. Brunelli, D. Lacroix, Flow perfusion rate modulates cell deposition onto scaffold substrate during cell seeding, Biomechanics and Modeling in Mechanobiology DOI 10.1007/s10237-017-0985-4.

[13] A. Campos Marin, T. Grossi, E. Bianchi, G. Dubini, D. Lacroix, 2D μ-Particle Tracking velocimetry and Computational Fluid Dynamics Study Within a 3D Porous Scaffold, Annals of Biomedical Engineering 45 (5) (2017) 1341–1351.

[14] A. Campos Marin, T. Grossi, E. Bianchi, G. Dubini, D. Lacroix, μ-particle tracking velocimetry and computational fluid dynamics study of cell seeding within a 3D porous scaffold, Journal of the Mechanical Behavior of Biomedical Materials 75 (2017) 463–469.

[15] A. Campos Marin, D. Lacroix, The inter-sample structural variability of regular tissue-engineered scaffolds significantly affects the micromechanical local cell environment, Interface Focus 5 (2015) 20140097–20140097.

[16] F. Galbusera, M. Cioffi, M. T. Raimondi, R. Pietrabissa, Computational modeling of combined cell population dynamics and oxygen transport in engineered tissue subject to interstitial perfusion, Computer Methods in Biomechanics and Biomedical Engineering 10 (2007) 279–287.

[17] M. Cioffi, J. Küffer, S. Ströbel, G. Dubini, I. Martin, D. Wendt, Computational evaluation of oxygen and shear stress distributions in 3D perfusion culture systems: Macro-scale and micro-structured models, Journal of Biomechanics 41 (2008) 2918–2925.

[18] B. Obradovic, J. H. Meldon, L. E. Freed, G. Vunjak-Novakovic, Glycosaminoglycan deposition in engineered cartilage: Experiments and mathematical model, AlChE Journal - The global home of chemical engineers 46 (2000) 1860–1871.

[19] K. A. Williams, S. Saini, T. M. Wick, Computational Fluid Dynamics Modeling of Steady-State Momentum and Mass Transport in a Bioreactor for Cartilage Tissue Engineering, Biotechnology Progress 18 (2002) 951–963.

[20] C. A. Chung, C. W. Yang, C. W. Chen, Analysis of cell growth and diffusion in a scaffold f or cartilage tissue engineering, Biotechnology and Bioengineering 94 (2006) 1138–1346.

[21] C. A. Chung, C. W. Yang, C. W. Chen, C. S. Tseng, Enhancement of cell growth in tissue-engineering constructs under direct perfusion: Modeling and simulation, Biotechnology and Bioengineering 97 (2007) 1603–1616.

[22] C. A. Chung, C. W. Yang, C. W. Chen, C. S. Tseng, A compact computational model for cell construct development in perfusion culture, Biotechnology and Bioengineering 99 (2008) 1535–1541.

[23] M. Ferroni, S. Giusti, D. Nascimento, A. Silva, F. Boschetti, A. Ahluwalia, Modeling the fluid-dynamics and oxygen consumption in a porous scaffold stimulated by cyclic squeeze pressure, Medical Engineering and Physics 38 (2016) 725–732.

[24] D. P. Byrne, D. Lacroix, J. A. Planell, D. J. Kelly, P. J. Prendergast, Simulation of tissue differentiation in a scaffold as a function of porosity, Young's modulus and dissolution rate: application of mechanobiological models in tissue engineering, Biomaterials 28 (36) (2007) 5544–5554.

[25] A. L. Olivares, E. Marsal, J. A. Planell, D. Lacroix, Finite element study of scaffold architecture design and culture conditions for tissue engineering, Biomaterials 30 (30) (2009) 6142–6149.

[26] J. L. Milan, J. A. Planell, D. Lacroix, Computational modelling of the mechanical environment of osteogenesis within a polylactic acid-calcium phosphate glass scaffold, Biomaterials 30 (25) (2009) 4219–4226.

[27] F. Zhao, T. J. Vaughan, L. M. McNamara, Multiscale fluid-structure interaction modelling to determine the mechanical stimulation of bone cells in a tissue engineered scaffold, Biomechanics and Modeling in Mechanobiology 14 (11) (2015) 231–243.

[28] A. P. G. Castro, D. Lacroix, Micromechanical study of the load transfer in a polycaprolactone-collagen hybrid scaffold when subjected to unconfined and confined compression, Biomechanics and Modeling in Mechanobiology 17 (2) (2018) 531–541.

[29] E. Kim, F. Guilak, M. A. Haider, The dynamic mechanical environment of the chondrocyte: A biphasic finite element model of cell-matrix interactions under cyclic compressive loading, Journal of Biomechanical Engineering 130 (6) (2008) 061009.

[30] L. Vikingsson, J. A. Gómez-Tejedor, G. Gallego Ferrer, J. L. Gómez Ribelles, An experimental fatigue study of a porous scaffold for the regeneration of articular cartilage, Journal of Biomechanics 48 (2015) 1310–1317.

[31] K. W. Li, A. K. Williamson, A. S. Wang, R. L. Sah, Growth responses of cartilage to static and dynamic compression, Clinical Orthopaedics and Related Research 391 (2001) S34–S48.

[32] M. D. Buschmann, Y. J. Kim, M. Wong, E. Frank, E. B. Hunziker, A. J. Grodzinsky, Stimulation of aggrecan synthesis in cartilage explants by cyclic loading is localized to regions of high interstitial fluid flow, Archives of Biochemistry and Biophysics 366 (1) (1999) 1–7.

[33] K. Sauerland, R. X. Raiss, J. Steinmeyer, Proteoglycan metabolism and viability of articular cartilage explants as modulated by the frequency of intermittent loading, Osteoarthritis and Cartilage 11 (5) (2003) 343–350.

[34] E. J. Blain, S. J. Gilbert, R. J. Wardale, S. J. Capper, D. J. Mason, V. C. Duance, Up-regulation of matrix metalloproteinase expression and activation following cyclical compressive loading of articular cartilage in vitro, Archives of Biochemistry and Biophysics 396 (1) (2001) 49–55.

[35] R. L. Mauck, S. L. Seyhan, G. A. Ateshian, C. T. Hung, Influence of seeding density and dynamic deformational loading on the developing structure/function relationships of chondrocyte-seeded agarose hydrogels, Annals of Biomedical Engineering 30 (8) (2002) 1046–1056.

[36] T. T. Chowdhury, D. L. Bader, J. C. Shelton, D. A. Lee, Temporal regulation of chondrocyte metabolism in agarose constructs subjected to dynamic compression, Archives of Biochemistry and Biophysics 417 (1) (2003) 105–111.

[37] A. J. Grodzinsky, M. E. Levenston, M. Jin, E. H. Frank, Cartilage tissue remodeling in response to mechanical forces, Annual Review of Biomedical Engineering 2 (2000) 691–713.

[38] S. W. Verbruggen, T. J. Vaughan, L. M. McNamara, Fluid flow in the osteocyte mechanical environment: a fluid-structure interaction approach, Biomechanics and Modeling in Mechanobiology 13 (2014) 85–97.

[39] E. Birmingham, J. A. Grogan, G. L. Niebur, L. M. McNamara, P. E. McHugh, Computational Modelling of the Mechanics of Trabecular Bone and Marrow Using Fluid Structure Interaction Techniques, Annals of Biomedical Engineering 41 (4) (2013) 814–826.

[40] T. J. Vaughan, M. G. Haugh, L. M. McNamara, A fluid-structure interaction model to characterize bone cell stimulation in parallel-plate flow chamber systems, Journal of Royal Society of Interface 10 (2013) 20120900.

[41] P. Yu, T. S. Lee, Y. Zeng, H. T. Low, A numerical analysis of effects of vortex breakdown on oxygen transport in a micro-bioreactor, International Communications in Heat and Mass Transfer 35 (2008) 1141–1146.

[42] P. Yu, Y. Zeng, T. S. Lee, H. T. Low, A numerical analysis of cell density effect on oxygen transport in a micro-bioreactor with a tissue engineering scaffold, International Communications in Heat and Mass Transfer 36 (2009) 569–573.

[43] P. Yu, T. S. Lee, Y. Zeng, H. T. Low, Fluid dynamics and oxygen transport in a micro-bioreactor with a tissue engineering scaffold, International Journal of Heat and Mass Transfer 52 (1-2) (2009) 316–327.

[44] A. R. Jackson, T. Y. Yuan, C. Y. Huang, M. D. Brown, W. Y. Gu, Nutrient Transport In Human Annulus Fibrosus Is Affected By Compressive Strain And Anisotropy, Annals of Biomedical Engineering 40 (12) (2017) 2551–2558.

[45] Y. F. Wang, C. M. Barrera, E. A. Dauer, W. Gu, F. Andreopoulos, C. Y. C. Huanga, Systematic characterization of porosity and mass transport and mechanical properties of porous polyurethane scaffolds, Journal of the Mechanical Behavior of Biomedical Materials 65 (2017) 657–664.

[46] M. G. Li, X. Y. Tian, X. B. Chen, Modeling of flow rate, pore size, and porosity for the dispensing-based tissue scaffolds fabrication, Journal of Manufacturing Science and Engineering 131 (3) (2009) 034501.

[47] X. B. Chen, M. G. Li, H. Ke, Modeling of the Flow Rate in the Dispensing-Based Process for Fabricating Tissue Scaffolds, Journal of Manufacturing Science and Engineering 130 (2) (2008) 021003.

[48] C. Sandino, D. Lacroix, A dynamical study of the mechanical stimuli and tissue differentiation within a CaP scaffold based on micro-CT finite element models, Biomechanics and Modeling in Mechanobiology 10 (2011) 565–576.

[49] I. Liao, F. T. Moutos, B. T. Estes, X. Zhao, F. Guilak, Composite three-dimensional woven scaffolds with interpenetrating network hydrogels to create functional synthetic articular cartilage, Advanced Functional Materials 23 (2013) 5833–5839.

[50] F. You, X. Wu, N. Zhu, M. Lei, B. F. Eames, X. B. Chen, 3D Printing of Porous Cell-Laden Hydrogel Constructs for Potential Applications in Cartilage Tissue Engineering, ACS Biomaterials Science & Engineering 2 (2016) 1200–1210.

[51] F. Eckstein, B. Lemberger, C. Gratzke, M. Hudelmaier, C. Glaser, K. H. Englmeier, M. Reiser, In vivo cartilage deformation after different types of activity and its dependence on physical training status, Annals of the Rheumatic Diseases 64 (2005) 291–295.

[52] ADINA, Theory and Modeling Guide, ADINA *R&D* Inc., Watertown, MA, USA.

[53] D. Lacroix, A. Chateau, M. P. Ginebra, J. A. Planell, Micro-finite element models of bone tissue-engineering scaffolds, Biomaterials 27 (2006) 5326–5334.

Tables

Table 1

Nomenclature of the scaffold samples as a function of the controlled parameters Y and D.

Y \ D	$0.2[mm]$	$0.3[mm]$	$0.4[mm]$
$0.5[mm]$	SC 1-1	SC 1-2	SC 1-3
$0.7[mm]$	SC 2-1	SC 2-2	SC 2-3
$0.9[mm]$	SC 3-1	SC 3-2	SC 3-3

Table 2

Geometrical dimensions and porosity of the scaffolds.

Y \ D	$0.2[mm]$		$0.3[mm]$		$0.4[mm]$	
	h_z $[mm]$	$\epsilon[\%]$	h_z $[mm]$	ϵ $[\%]$	h_z $[mm]$	ϵ $[\%]$
$0.5[mm]$	0.179	66.9	0.268	49.9	0.358	34
$0.7[mm]$	0.17	75.8	0.255	63.9	0.34	51.7
$0.9[mm]$	0.16	80.6	0.24	71.3	0.32	61.2

Table 3

Computed pressure drops (in $[mPa]$) as a function of the controlled parameters Y (in $[mm]$) and D (in $[mm]$) of the different scaffolds.

Y \ D	$0.2[mm]$	$0.3[mm]$	$0.4[mm]$
$0.5[mm]$	96.16	144.89	227.523
$0.7[mm]$	9.87	22.65	40.673
$0.9[mm]$	0.0854	1.669	11.919

Figures

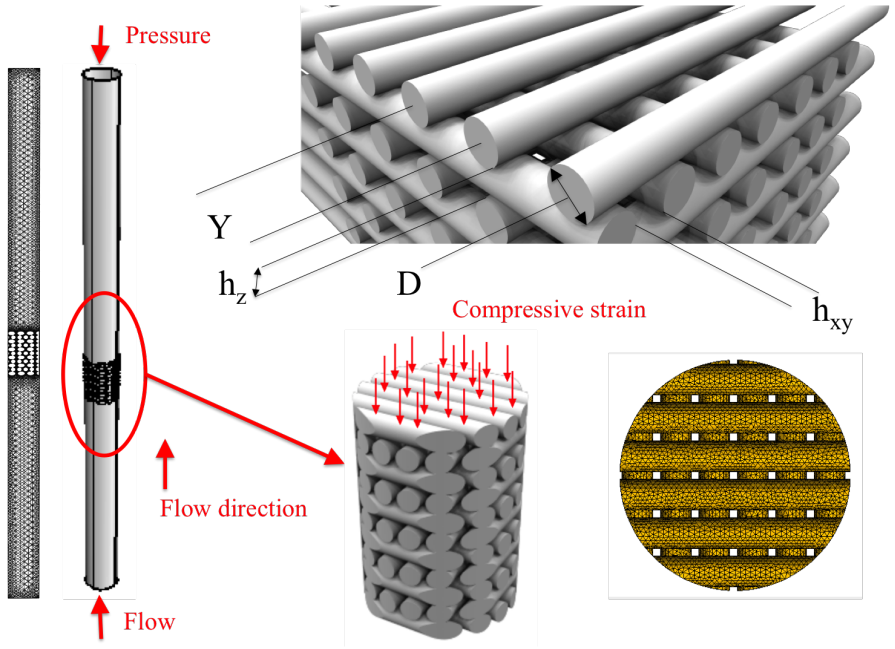

Fig. 1. Geometry of the scaffold $SC1-3$ with controllable parameters and mesh details.

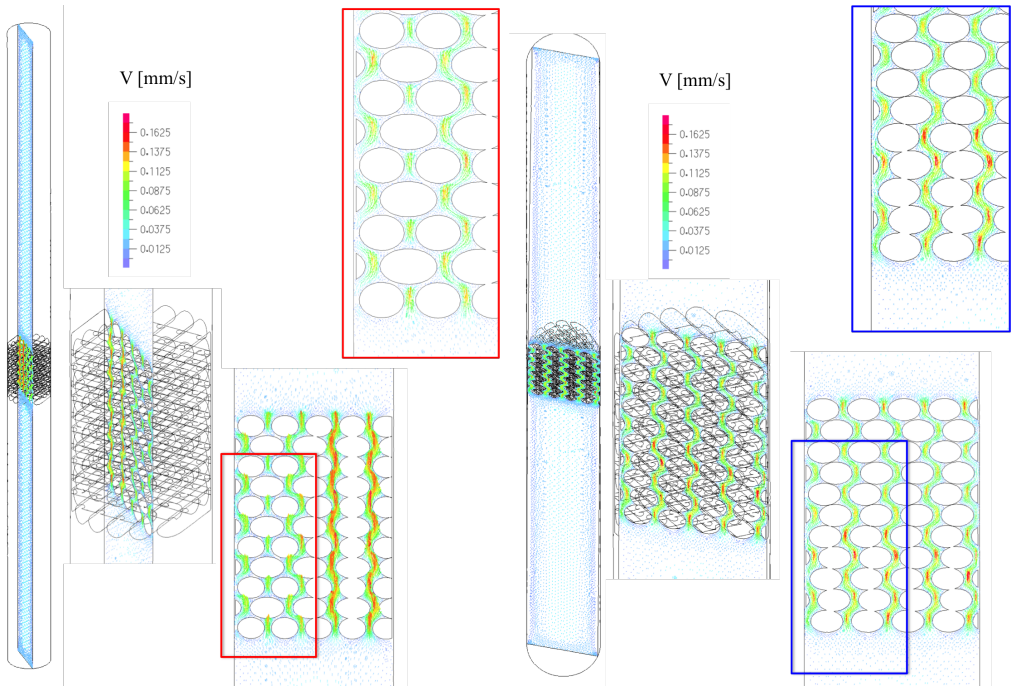

(a) (b)

Fig. 2. Projected velocity arrows representing for different cut planes the fluid motion inside the scaffold architecture $SC1-3$.

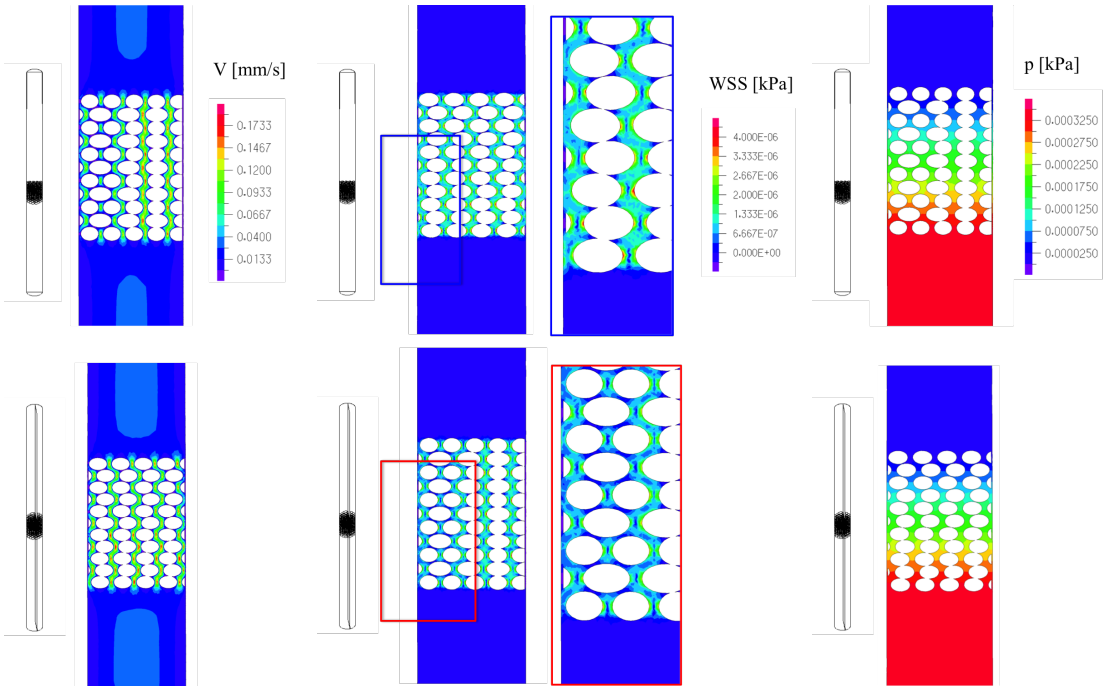

(a) (b) (c)

Fig. 3. Velocity magnitude contours (in $[mm/s]$) within the scaffold (a) in different cut planes, WSS (in $[kPa]$) (b) and pressure distribution (in $[kPa]$) (c) within the scaffold $SC1-3$.

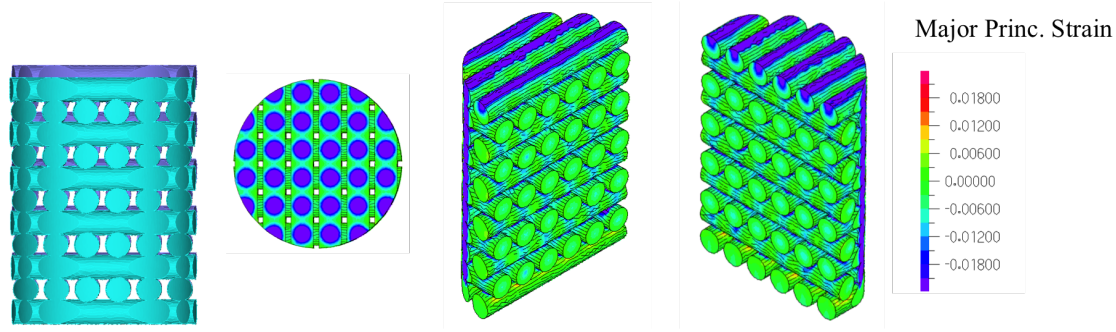

(a) (b)

Fig. 4. Undeformed (colored in purple) vs. deformed shape (colored in light blue) of the scaffold $SC1-3$ (a). Major principal strain distribution of the scaffold $SC1-3$ at selected cutting planes (b).

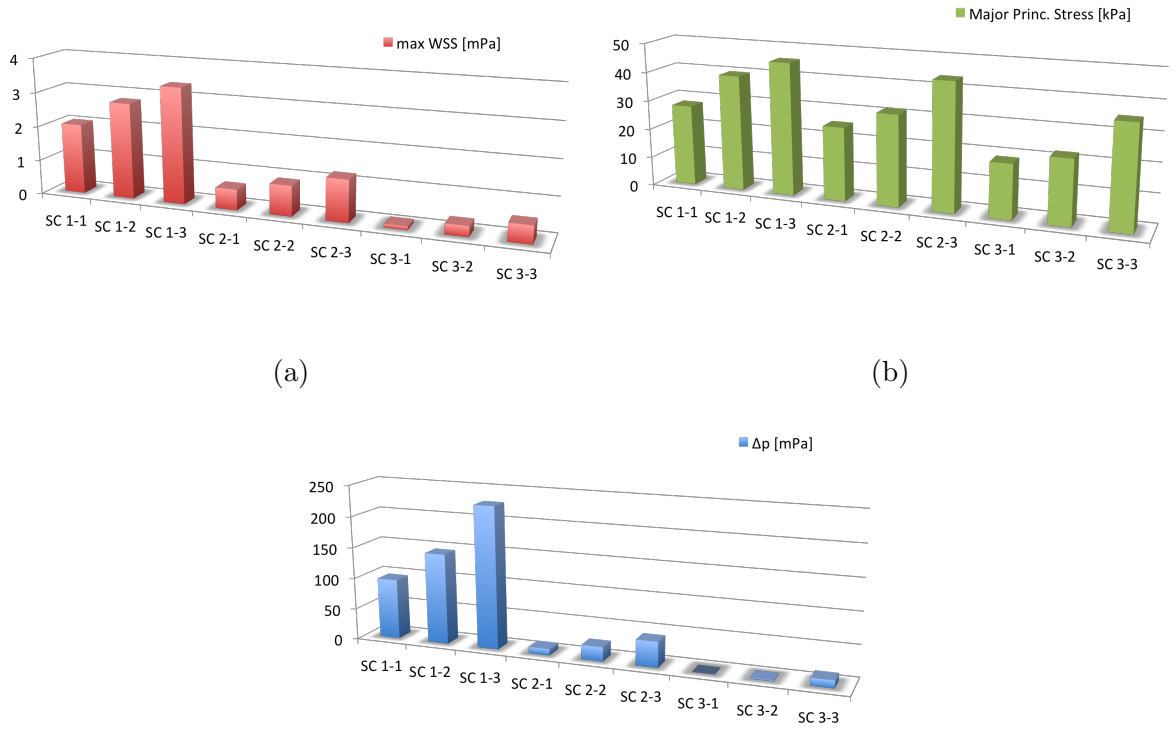

(a) (b)

(c)

Fig. 5. Maximum wall shear stress (in $[mPa]$) (a), absolute values of the compressive major principal stress (in $[kPa]$) (b) and pressure drop (in $[mPa]$) (c) within the different scaffolds.

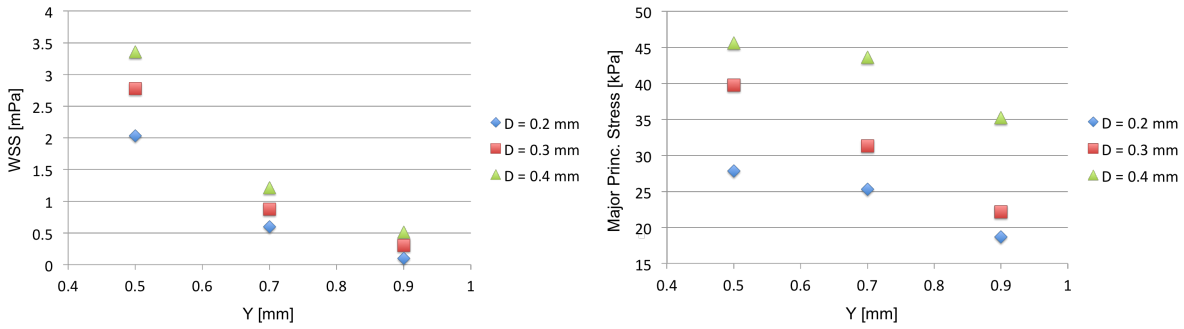

(a) (b)

Fig. 6. Maximum wall shear stress variation (in $[mPa]$) versus D (in $[mm]$) and Y (in $[mm]$) (a) and absolute value of the compressive maximum principal stress variation (in $[kPa]$) versus D (in $[mm]$) and Y (in $[mm]$) (b).

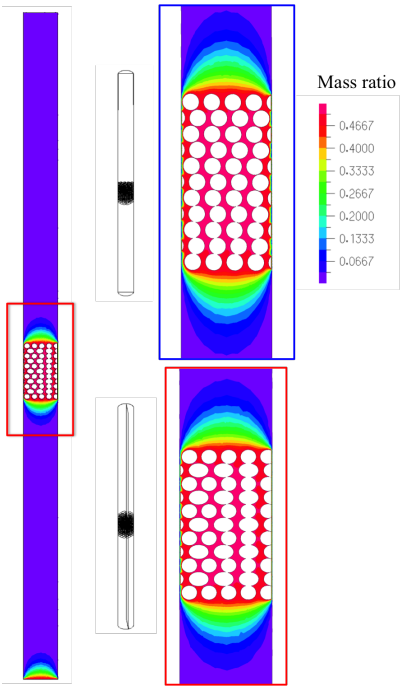

Fig. 7. Distribution of the nutrient concentration within the scaffold $SC1-3$.